Tanzania Journal of Science 49(5): 1138-1150, 2023
ISSN 0856-1761, e-ISSN 2507-7961

Synthesis of Template-free Flower-like ZnO Nanorods using a Simple Chemical Bath Technique

Benard S. Mwankemwa *
Physics Department, College of Natural and Mathematical Sciences, University of Dodoma, P. O. Box 338, Dodoma, Tanzania
** Corresponding Author.* E-mail address: *benard198028@gmail.com*
Received 25 Sept 2023, Revised 17 Nov 2023, Accepted 12 Dec 2023, Published Jan 2024
https://dx.doi.org/10.4314/tjs.v49i5.16

Abstract

Flower-like ZnO nanorods were successfully synthesised using a template-free, low-temperature chemical bath deposition method. The effects of growth time on the structural, morphological, and vibrational properties of flower-like zinc oxide were investigated. X-ray diffraction (XRD) and scanning electron microscopy (SEM) indicated that the crystallite size and density of flower-like ZnO nanorods increased with increasing growth time. Raman spectroscopy confirmed the existence of specific Raman modes that correspond to the wurtzite structure of ZnO. In addition, Raman measurements revealed that increased growth time increases the Raman modes intensity of the flower-like ZnO nanorods. Moreover, the measurements of the Au/ZnO nanorods/FTO Schottky diode showed that all devices functioned as Schottky diodes and rectifying; however, their ideality factor was greater than 1. In addition to the ideality factor, the Schottky barrier height was calculated and slightly increased with growth time. The values of Schottky barrier height obtained were 0.502 eV, 0.523 eV, 0.516 eV and 0.529 eV for samples grown at 1, 2, 3 and 4 h, respectively.

Keywords: ZnO nanorods, Surface morphology, Schottky diode, rectification ratio

Introduction

Zinc oxide (ZnO) nanorods have been extensively studied because of their characteristics as an n-type semiconductor that has a broad and direct band gap of 3.37 eV, and they possess a considerable excitonic binding energy of 60 meV at room temperature (Azimirad et al. 2014, Shabannia and Abu Hassan 2014, Das et al. 2022). They are gaining popularity due to their significant effective surface area and high surface-to-volume ratio and are proving useful in various fields, such as ultraviolet (UV) lasers, light emitting diode (LED) lights, surface acoustic wave devices, piezoelectric sensors, nanogenerators, and solar cells (Kim et al. 2014, Mohamed et al. 2016, Mohammad et al. 2020, Mwankemwa et al. 2022, Yao et al. 2022).

There are several methods for synthesising ZnO nanorods, such as chemical bath deposition (CBD) (Malevu et al. 2019, Ungula et al. 2022), electrochemical deposition (Hames et al. 2010, Solís et al. 2020), vapour phase technique (Vallejos et al. 2016, Kong et al. 2018, Kennedy et al. 2019), aerosol-assisted chemical vapour deposition (AACVD) (Abd et al. 2014, Jiamprasertboon et al. 2019), and Atomic Layer Deposition (ALD) (Nandanapalli and Mudusu, 2018, Karajz et al. 2022). CBD is a user-friendly method for the synthesis of flower-like ZnO nanorods when compared to other methods. It is a low-temperature method that is cheap and capable of large-scale production. It also offers versatility in terms of substrates, accommodating both conducting and non-conducting substrates. This is a key advantage because other methods are frequently restricted to specific substrate types. Furthermore, CBD does not require any metal catalyst, which might be expensive, as well as no potential severe health and environmental dangers (Xu and Wang, 2011, Farhat et al., 2015, Rana et al. 2015, Yuan, 2015). This technique can accurately manipulate the nanorods' size, shape, and density, thus creating customised properties that suit particular purposes. Strano et al. (2019) utilised CBD to synthesise ZnO microflowers. The addition of ammonium fluoride to the bath was the crucial component that led to the formation of the microflowers, which consisted of extremely thin sheets arranged in a spherical pattern. Babayevska et al. (2022) have prepared hierarchical flower-like structures and tetrapods of ZnO using the solvothermal reaction and oxidative metal vapour transport method, respectively. The SEM image has confirmed the formation of the hierarchical flower-like (peony) structure, where all individual particles have a spherical shape. Their study has also reported on the tetrapods, which were well-faceted with four uniform hexagonal-shaped legs connected to a central nucleus. According to a study by Shabannia (2015), the ZnO nanorods prepared using laboratory oven-assisted CBD on porous silicon substrates were examined to determine the effect of growth time on their properties. The results indicated that as the growth time increased, the diameter and length of the ZnO nanorods increased. Zhitao et al. (2013) investigated the effect of ammonia on the growth time of ZnO nanorods prepared using an improved hydrothermal technique in a closed bottle put in an oven. According to their report, when the conditions were optimised, the length of ZnO nanowires increased rapidly and primarily linearly as the growth time progressed. When deposited on a patterned glass substrate, they further obtained flower-like nanorod arrays emanating from a single point. Unlike previous studies that resulted in nanorods growing vertically perpendicular to the substrate and using patterned substrates, this study produced flower-like ZnO nanorod bundles originating from a single point and deposited on unpatterned substrates. It adopted a template-free low-temperature chemical bath method to evaluate the impacts of growth time on the ZnO nanorods. Other synthesis parameters such as pH, solution concentration and temperature were maintained constant. This study, therefore, presents significant results regarding the structural, morphological, and vibrational characteristics of flower-like ZnO nanorods. In addition, current-voltage (*I*–*V*) measurements were used to study the electrical properties of the gold (Au)/ZnO nanorods/FTO Schottky diodes structure. By doing many tests on different Schottky contact points, it was discovered that increasing the growth time enhanced the Schottky diodes' rectification behaviour. The samples grown for 4 h showed three orders of magnitude greater rectification ratios than those grown for 1 h, indicating increased device performance. It should be noted that the experiments were conducted in an empty beaker placed in a water bath without using a laboratory oven, autoclave, or microwave oven.

Figure 1 shows a schematic diagram of the setup used for the experiments with the schematic of obtained ZnO nanorods.

Materials and Methods

Sample preparation

This study dissolved 2.5000 g of zinc acetate dehydrate from Sigma-Aldrich in 40 ml of ethanol and stirred at 500 rpm for 40 minutes at 50 °C. Afterwards, 1.2 grams of monoethanolamine (MEA) from Sigma-Aldrich were added to the reaction mixture and stirred at the same rate and temperature for 2 h. A homogenous and transparent seed solution was obtained and then aged for 24 h. Before the growth of the ZnO thin films seed layer, Fluorine-doped Tin Oxide (FTO), Merck with surface resistivity of 2 Ω/cm glass substrates (2 cm × 1 cm × 2.2 mm) were systematically cleaned using a warm soap solution and rinsed with distilled water. After that, substrates were sonicated in acetone, ethanol and distilled water for 3 minutes each. Before seed layer deposition, the FTO substrates were wrapped at the edge with a non-sticking tape to reserve the same for contact. ZnO seed layer were therefore spin-coated on the cleaned glass substrates at a spinning rate of 2000 rpm for 1 minute and then dried on a hot plate at 100 °C for 5 minutes. The process was repeated three times, and eventually, the obtained ZnO thin film was utilised as the seed layer for the growth of ZnO nanorods. The growth of ZnO nanorods on the seeded FTO glass substrates was performed using the CBD technique (Figure 1). The recipe for producing ZnO nanorods involves dissolving equimolar amounts (0.025 M) of zinc nitrate hexahydrate and hexamethylenetetramine from Sigma-Aldrich in distilled water. The seeded FTO glass substrates were placed in a 500 ml beaker filled with a 7.9 pH growth solution, with the seed layer facing sideways. Low-cost nylon non-releasable cable ties, 30 cm in length, were used to hold the substrates. The unseeded sides were covered using non-sticking tape to avoid depositing on either side of the substrates. The beaker with growth solution was placed inside a 1000 ml beaker with preheated water maintained at a constant temperature of 65 °C. The mixture was stirred continuously at a rate of 300 rpm. The level of the water and growth solution maintained constant throughout the experiment. The experiments were done for 1, 2, 3 and 4 h to investigate the effect of growth time on the synthesised flower-like ZnO nanorods. At the end of the experiment, the samples were removed from the growth solution, thoroughly rinsed with distilled water to remove any residual salts, and dried in air for 15 minutes. The resistive evaporation was then employed to deposit gold (Au) metal of approximately 0.8 mm in diameter at a pressure of 4×10^{-4} mbar. This was done using a circular shadow mask to create FTO/ZnO nanorods/Au Schottky diodes. In this arrangement, Au served as the Schottky contact, while the ohmic contact was achieved using FTO (previously covered).

Sample characterisation

X-ray diffraction XRD evaluated the crystallographic properties of the flower-like ZnO nanorods using PANalytical X'Pert Pro powder X-ray diffraction with Cu-Kα radiation operated at a voltage of 45 kV and a current of 40 mA. The surface morphology of the prepared flower-like ZnO nanorods was studied using Field emission scanning electron microscopy (FE-SEM). Raman studies were conducted using 5 Horiba Jobin Yvon micro Raman with excitation wavelength λ = 514.5 nm in the range 50 cm^{-1} to –1000 cm^{-1} to investigate the vibrational properties of the synthesised flower-like ZnO nanorods. Current-voltage (I–V) properties of the Schottky diode were measured in the dark and at RT using Keithley 4200 semiconductor parameter analyser.

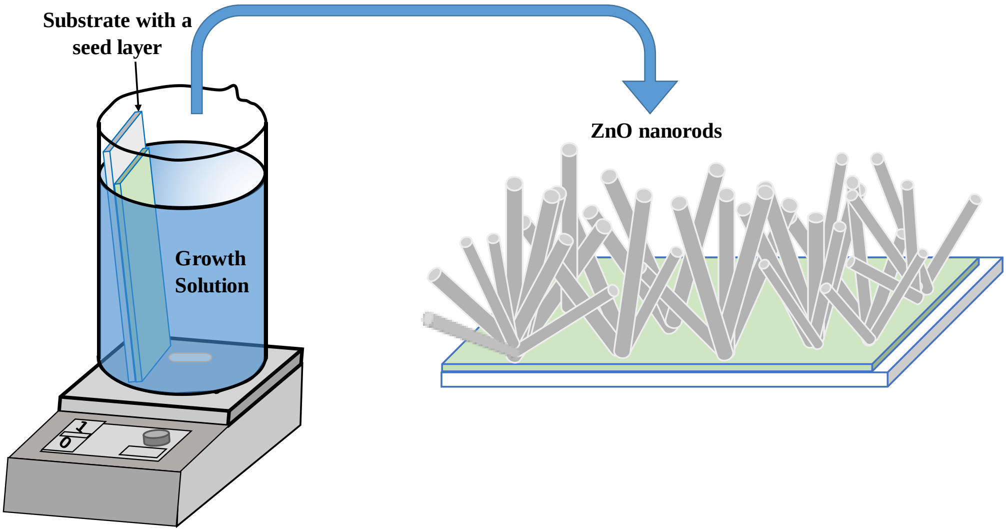

Figure 1: Schematic illustration of the setup for CBD employed in this study and ZnO nanorods.

Results and Discussion

Structural characterisation

The XRD patterns in Figure 2 show highly oriented peaks of ZnO nanorods grown on seeded soda lime glass substrates at different growth times. Regardless of the growth time, the significant peaks in the 2θ range of 20º to 75º for the samples are indexed to the hexagonal wurtzite structure of ZnO (space group *P*6$_3$*mc*), which agrees with JCPDS card number 36-1451. The patterns indicate preferred orientation along the (002) direction as the intensities of the (002) planes differed significantly from those of the (100) and (101) planes, suggesting that the deposited flower-like ZnO nanorods are highly *c*-axis oriented (Pereira et al. 2013, Gaddam et al. 2015, Rana et al. 2015). Additional peaks along the (102), (110), (103), (112) and (004) directions were also observed. All these peaks belongs to the wurtzite structure of ZnO and thus proved that the obtained flower-like ZnO nanorods are free from other phases. The present study demonstrates that peak intensities increase as the growth time increases, indicating a higher degree of crystallinity in the flower-like ZnO nanorods with longer growth times. These results compare well with those reported by Liu and co-workers (Liu et al. 2011).

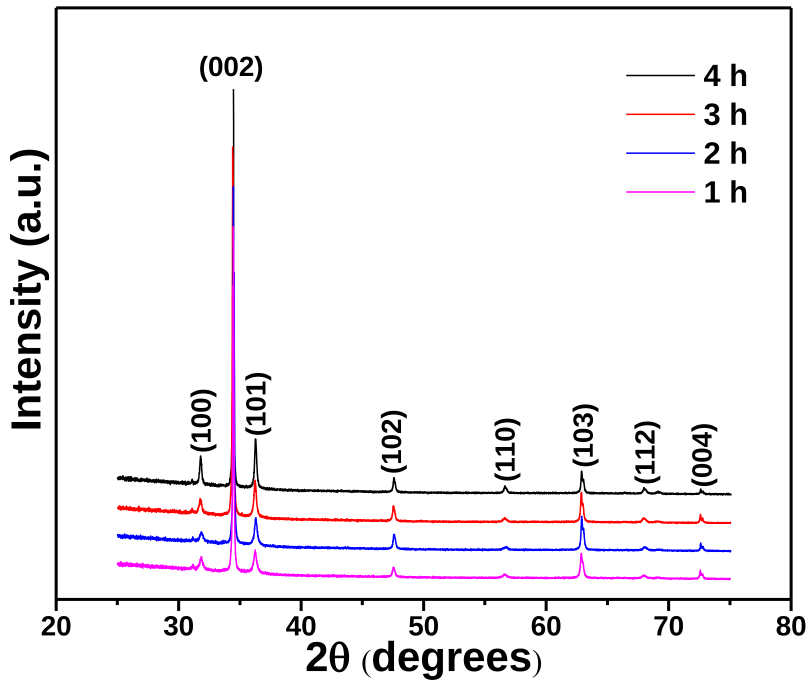

Figure 2: XRD patterns of ZnO nanorods prepared at different time intervals.

The flower-like ZnO nanorods exhibited good crystal quality as seen from the clear and sharp diffraction peaks. The crystallite size (D) was determined using Scherer's equation:

$$D = \frac{0.9\lambda}{\beta \cos\theta} \qquad (1)$$

where, λ is the wavelength of X-ray radiation of the incident Cu Kα radiation (1.540 Å), θ is the Braggs angle, and β is the Full Width at Half Maximum (FWHM) of the dominant peak. The most prominent diffraction peak along the (002) direction was observed in all samples. Based on this plane, the crystallite size was calculated and the findings are presented in Table 1. The results show that crystallite size increased with increasing growth time. The lattice constants *a* and *c* were calculated using Bragg's law:

$$a = \sqrt{\frac{1}{3}}\frac{\lambda}{\sin\theta} \qquad (2)$$

$$c = \frac{\lambda}{\sin\theta} \qquad (3)$$

In the present study, however, the flower-like ZnO nanorods lattice constants (shown in Table 1) are lower than the standard values (compared from a and c of ZnO bulk which are 3.2498 Å and 5.2066 Å, respectively). This could be because the samples were dried at lower temperatures without undergoing post-annealing treatment at higher temperatures.

Table 1: The effect of growth time on crystallite sizes and lattice parameters of the synthesised nanorods.

Growth time (h)	Lattice parameters			Average Crystallite size, *D* (nm)	Strain (ε) × 10^{-3}
	***a* (Å)**	***c* (Å)**	***c*/*a***		
1	3.2258	5.1692	1.6025	58.83	19.81
2	3.2310	5.1889	1.6059	59.35	20.02
3	3.2298	5.1893	1.6066	59.45	20.09
4	3.2381	5.1978	1.6052	60.64	20.16

Williamson and Hall (Rana et al. 2015) equation 4 was plotted in Figure 3 and used to estimate the strain induced in the flower-like ZnO nanorods as the effects of growth time.

$$\beta_{hkl} = \frac{0.9\lambda}{D\cos\theta} + 4\varepsilon\tan\theta \qquad (4)$$

where symbol ε represents induced strain, while the other symbols have their usual meanings as defined previously. A longer growth time has resulted in a higher strain, indicating that the flower-like ZnO nanorods experience compressive strain, as reported by Mosalagae et al. (2020).

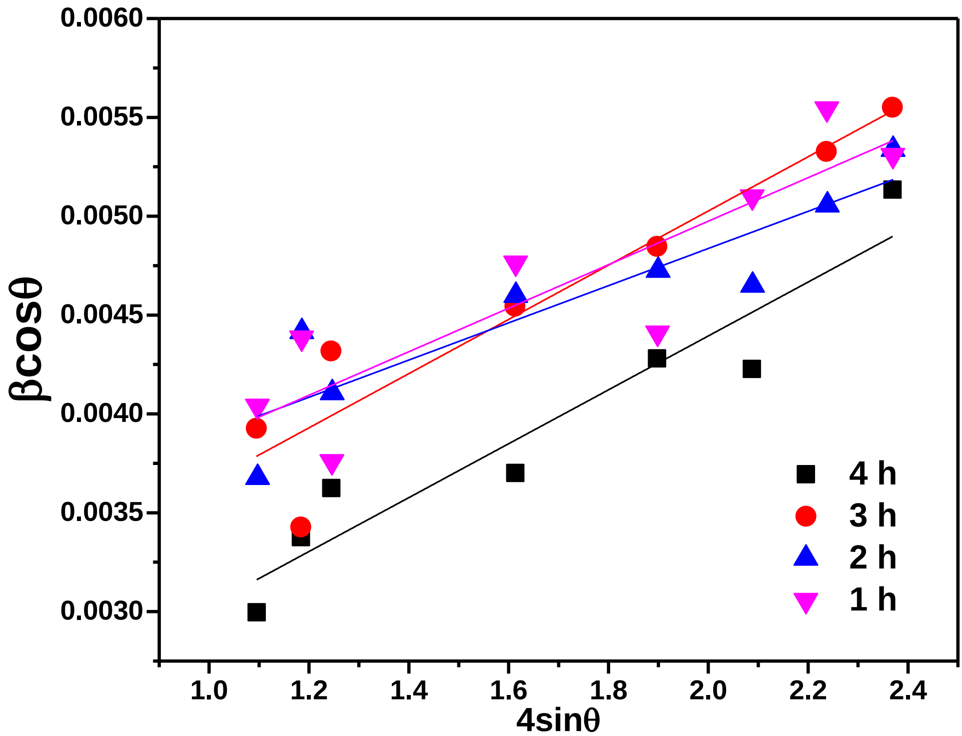

Figure 3: Williamson-Hall plot of ZnO nanorods prepared at different time intervals.

Surface morphology

The surface morphologies of the prepared flower-like ZnO nanorods at different growth durations are shown in Figure 4. Upon examining Figure 3, it is evident that the morphology of the nanorods undergoes various changes with increased growth time. As the growth time increases, the density of flower-like ZnO nanorods also increases. SEM micrographs of the sample synthesised for 4 h demonstrate more flower-like nanorods than the one prepared at 1 h. Thus, with longer growth times, more ZnO material is deposited on the substrate, increasing ZnO nanorods as well as the quality and alignment of ZnO nanorods. Shorter growth times typically result in shorter and sparser nanorods, while longer growth times lead to longer and denser nanorods. Nanorods with a preferential growth direction on a particular facet of interest can be obtained by considering proper growth parameters such as pH, growth time, temperature and seed layer thickness. According to a study conducted by Baruah and Dutta (2009), growth rates in both the lateral and longitudinal directions are greater in basic solutions than in acidic solutions. Their research indicated that acidic solutions had a slow growth rate, whereas basic solutions have a faster growth rate. In addition to that, a study by Liu and Gao (2015) demonstrated that, pH changes the distribution and density of nanorods, crystal sizes, and alignment. In this study, therefore, increased nanorods density on the substrate could be associated to the fact that the solution changed from acidic for the 1 h grown nanorods to basic for those grown for more than 1 h. By extending the growth time, the nanorods have more time to grow in length and fill up the available nucleation sites on the substrate. Furthermore, the arrangement of the nanorods can also be attributed to the diffusion-limited growth mechanism, where the available precursor concentration becomes the limiting factor for growth as the reaction progresses (Shabannia 2016).

Moreover, it is observed that shorter growth times lead to less aligned ZnO nanorods. However, as the growth time increases, the nanorods tend to align more uniformly and exhibit better orientation along a specific direction (Shabannia 2016). The diameter of ZnO nanorods can also be affected by growth time. It has been observed that initially, as the growth time increases, the diameter of the nanorods decreases. The decrease in the diameter is attributed to the competition between the lateral growth and vertical growth of the nanorods, as previously reported by Khayatian et al. (2017).

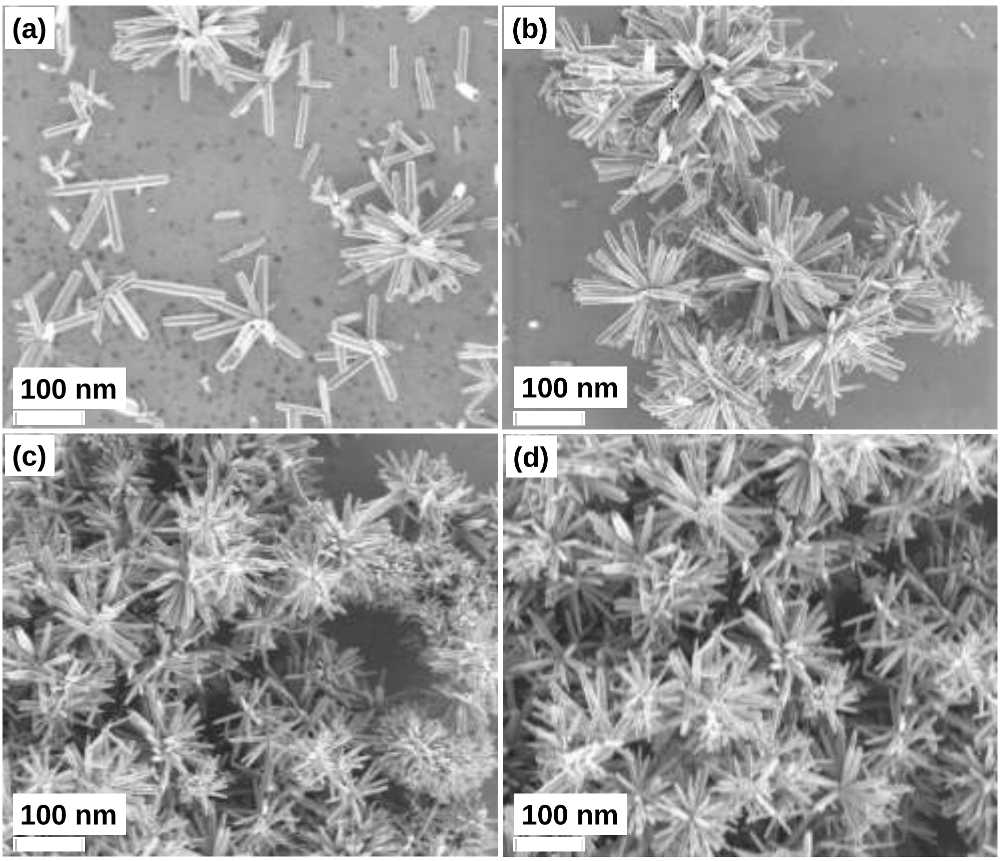

Figure 4: FESEM images of flower-like ZnO nanorods as a function of growth time: (a) 1 h, (b) 2 h, (c) 3 h and (d) 4 h

Raman studies

Raman studies were carried out to investigate the impact of growth time on the vibration modes of flower-like ZnO nanorods. In the Wurtzite structure of ZnO, there are phonon modes from $2E_1$, $2E_2$, $2A_1$, and $2B_1$. The modes with B_1 symmetry are silent, meaning they are Raman inactive. Polar A_1 and E_1 phonon modes are further subdivided into two optical modes: transverse optical (TO) and longitudinal optical (LO), whereas non-polar E_2 is further subdivided into E_2 (high) and E_2 (low) (Das et al. 2015, Jaramillo et al. 2017, Strelchuk et al. 2017). The room-temperature Raman spectra of flower-like ZnO nanorods are shown in Figure 5. The Raman modes that were detected are as follows: E_2 (low) at 99.22 cm^{-1}, a weak $2E_2$ mode at 201.92 cm^{-1}, E_2 (high) – E_2 (low) at approximately 332.14 cm^{-1}, A_1 (TO) at 379.99 cm^{-1}, E_2 (high) at 437.09 cm^{-1}, and E_1 (LO) at 581.92 cm^{-1}. Upon observation, it is evident that the Raman spectra of the samples display a heightened intensity and sharpness of the E_2 (low) and E_2 (high) optical phonon peaks at 99.22 cm^{-1} and 437.09 cm^{-1}, which correlate to the vibrations of zinc sub-lattice and oxygen atoms, respectively. It should be noted that the E_2 modes determine the wurtzite structure of ZnO, and their intensity determines the crystallinity of the ZnO. In the present study, the E_2 modes have the highest intensity and increase with growth time, indicating an improved crystalline nature, as indicated by XRD.

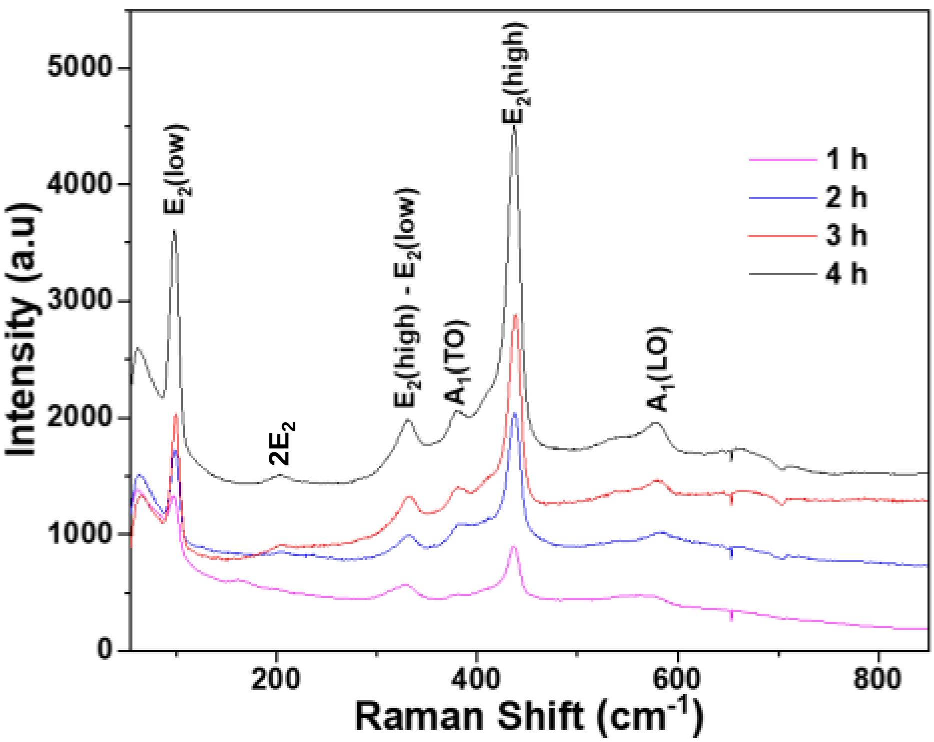

Figure 5: Room temperature Raman spectra of flower-like ZnO nanorods as a function of growth time.

In the present study, when growth time increases, the Raman peaks become more pronounced, indicating an enhancement in crystallinity, as reported by Mosalagae et al. (2020). However, Raman modes slightly shift to lower frequency as the growth time increases. Nevertheless, the wurtzite crystal structure of the ZnO lattice remained unaltered. Additionally, a polar peak at E_1 (LO) at 581.92 intensity increased as growth time increased, as shown in Figure 5. The fitting of the E_2 (high) provided the full width at half maximum of the four samples. The full width at half maximum (FWHM) values were slightly different for the samples grown at 1 h, 2 h, 3 h, and 4 h, being 8.4172 cm^{-1}, 8.6172 cm^{-1}, 8.3618 cm^{-1}, and 8.2889 cm^{-1}, respectively. This variation could be associated with the density of the nanorods. It is known that Raman peaks position and profile depend on several factors such as crystallisation, structural disorder, crystal defects, residual stress, and density of ZnO nanorods. Therefore, the observed slight change in FWHM could be attributed to the density of the nanorods. Raman spectroscopy confirmed the existence of specific Raman modes that correspond to particular wavenumbers, verifying the presence of the hexagonal ZnO phase.

The room temperature *I–V* characteristics under dark conditions of the flower-like ZnO nanorods Schottky diode having a structure FTO/ZnO nanorods/Au are displayed in a semi-log scale in Figure 6. As the forward and reverse current curves are anti-symmetric, all the devices are rectifying and thus function as Schottky diodes, as reported by Faraz et al. (2012). The graphs show an improved rectification behaviour, which is directly related to longer growth times. The Schottky diodes rectifying behaviour improved, as evidenced by the roughly two orders of magnitude difference between the forward and reverse current measured at ±1 V applied voltage in the case of Schottky diodes fabricated on the 3 h and 4 h flower-like ZnO nanorods. The results demonstrated that growth time affects rectifying properties due to the increased ZnO nanorod density, opening up paths for electrons to reach the substrate (Gonzalez-Valls and Lira-Cantu 2009).

Electrical characterisation

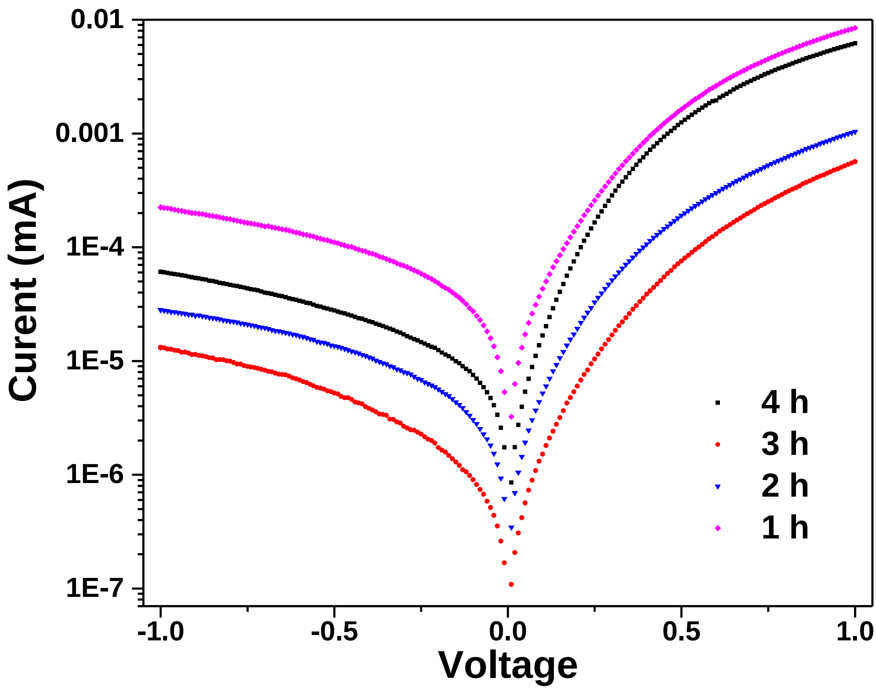

Figure 6: Semi logarithmic I–V characteristics of FTO /ZnO/Au Schottky diode measured in the dark.

The flower-like ZnO nanorods beneath the Au metal could be considered a series of individual Schottky diodes connected in parallel. Schottky barrier height Φ_{B0}, ideality factor n, and reverse saturation current I_0 (shown in Table 2) were estimated from I–V measurements using Sze's standard Thermionic emission theory of the Schottky diode (Sze, 1979). The ideality factor defines how well a diode conforms to pure thermionic emission. Any value larger than one implies non-ideal diode performance, demonstrating that thermionic emission is not the major transport mechanism. In the present study, all samples have an ideality factor greater than 1. The poor performance of the fabricated Schottky diodes can be attributed to several factors, such as unevenness on their top surface, high resistance in series, uneven distribution of charges at the interface, voltage drop across the M/S junction and the presence of defects and leakage currents caused by high levels of recombination (Breitenstein et al. 2009, Kathalingam et al. 2012, Narayanan, Ganesh, and Karthigeyan 2016, Singh et al. 2017). Furthermore, samples were used as-deposited; thus, oxygen vacancies may be present on the as-deposited ZnO surface, acting as donor-like centres, resulting in a significant leakage current tunnelling from Au into the as-deposited ZnO structure, as reported by Hwang and Hong (2021). The reverse saturation current I_0 in the present study is in the order of 10^{-6}, indicating that even when the diode is switched off, a small current continues to flow through the diode. Again, the larger the reverse current, the more problems can arise in some applications where small amounts of current must be monitored.

Table 2: Electrical parameters of FTO/ZnO nanorods/Au Schottky diode at different growth times.

Growth time (h)	**Saturation current (I_0, A) × 10^{-6}**	**Ideality facto (n)**	**Barrier height (Φ_{B0}, eV)**
1	4.35	4.2	0.502
2	4.29	4.2	0.523
3	4.17	4.1	0.516
4	4.32	4.1	0.529

Conclusion

Template-free flower-like ZnO nanorods were successfully synthesised using a simple CBD technique. The effect of growth time on the structural, morphology and vibrational properties was investigated. XRD analysis confirms the synthesised flower-like ZnO nanorods are in the (002) plane, and crystallite size increased with increasing growth time. SEM results indicated that the density and alignment of flower-like ZnO nanorods highly depend on the growth time. Raman measurement revealed that growth time affects the vibration properties of the synthesised flower-like ZnO nanorods. As the growth time increases, the non-polar E_2 peaks become more intense, showing an improvement in crystallinity. Additionally, the peaks shift slightly towards lower frequencies, suggesting the occurrence of tensile strain. The results demonstrated that a simple and cost-effective CBD technique is favourable for synthesising template-free flower-like ZnO nanorods. In this particular study, the growth time was altered while maintaining consistency with precursor concentration, temperature and pH. The I–V characteristics of the diodes display rectifying properties as demonstrated by the non-symmetric forward and reverse current curves. The electrical characterisation of the FTO/ZnO nanorods/Au Schottky diode showed that all the devices were rectifying and functioned as Schottky diodes with an ideality factor greater than 1. The diode rectification behaviour gradually improved with increased growth time. In conclusion, growth time considerably influenced the quality of ZnO nanorods, and the results are comparable with previous results using other methods.

Declaration of competing interest

The author declares no known competing financial interests or personal relationships in this work.

Acknowledgements

The financial assistance of the University of Dodoma and The World Academy of Sciences (TWAS), Italy, under its Research Grants Scheme Grant Number 20-091 RG/PHYS/AF/AC I and Swedish International Development Cooperation Agency (Sida) are grateful for their financial support. The author acknowledges Dr Thembinkosi Donald Malevu for his support in XRD, SEM and electrical measurement.

References

Abd Aziz SNQA, Pung SY and Lockman Z 2014 Growth of Fe-doped ZnO nanorods using aerosol-assisted chemical vapour deposition via in situ doping. *App. Phys. A.* 116 (4): 1801-1811.

Azimirad R, Khayatian A, Safa S, Almasi KM 2014 Enhancing photoresponsivity of ultra violet photodetectors based on Fe doped ZnO/ZnO shell/core nanorods. *J. Alloys Compd.* 615: 227–233.

Babayevska N, Przysiecka Ł, Iatsunskyi I, Nowaczyk G, Jarek M, Ewa Janiszewska E and Jurga S 2022 ZnO size and shape effect on antibacterial activity and cytotoxicity profile. *Sci. Rep.* 12:8148.

Baruah S and Dutta J 2009 pH-dependent growth of zinc oxide nanorods. *J. Crst. Growth* 311: 2549–2554.

Breitenstein O, Bauer J, Altermatt PP and Ramspeck K 2009 Influence of Defects on Solar Cell Characteristics. *Solid State Phenom.* 156–158 (1): 1–10.

Das S, Ghorai UK, Dey R, Ghosh CK and Pal M 2022 White Light Phosphorescence from ZnO Nanoparticles for White LED Applications. *New J. Chem.* 46 (36): 17585-17595.

Das R, Kumar A, Kumar Y, Sen S and Shirage PM 2015 Effect of Growth Temperature on the Optical Properties of ZnO Nanostructures Grown by Simple Hydrothermal Method. *RSC Advances* 5 (74): 60365–72.

Faraz SM, Willander M and Wahab Q 2012 Interface State Density Distribution in Au/n-ZnO Nanorods Schottky Diodes. *IOP Conference Series: Mater. Sci. Eng.* 34 (1).

Farhat OF, Halim MM, Abdullah MJ, Ali MKM and Allam NK 2015 Morphological and structural characterization of single-crystal ZnO nanorod arrays on flexible and non-flexible substrates. *Beilstein J. Nanotechnol.* 6: 720–725.

Gaddam V, Kumar RR, Parmar M, Nayak MM and Rajanna K 2015 Synthesis of ZnO Nanorods on a Flexible Phynox Alloy Substrate: Influence of Growth Temperature on Their Properties. *RSC Adv.* 5 (109): 89985–92.

Gonzalez-Valls I and Lira-Cantu M 2009 Vertically-Aligned Nanostructures of ZnO for Excitonic Solar Cells: A Review. *Energy Environ. Sci.* 2 (1): 19–34.

Hames Y. Alpaslan Z, Kösemen A, San SE and Yerli Y 2010 Electrochemically grown ZnO nanorods for hybrid solar cell applications. *Solar Energy.* 84: 426–431.

Hwang JD and Hong ZJ 2021 Enhancing the Schottky-barrier height by inserting a thin MgO layer between Au and annealed-ZnO. *Mater. Res. Bull.* 144: 111478

Jaramillo AF, Baez-Cruz R, Montoya LF, Medinam C, Pérez-Tijerina E, Salazar F, Rojas D and Melendrez MF 2017 Estimation of the Surface Interaction Mechanism of ZnO Nanoparticles Modified with Organosilane Groups by Raman Spectroscopy. *Ceram. Int.* 43 (15): 11838–47.

Jiamprasertboon A, Dixon S C, Sathasivam S, Powell M J, Lu Y, Siritanon T and Carmalt C J 2019 Low-Cost One-Step Fabrication of Highly Conductive ZnO:Cl Transparent Thin Films with Tunable Photocatalytic Properties via Aerosol-Assisted Chemical Vapor Deposition. *ACS Appl. Electron. Mater.* **2019** 1: (8), 1408-1417.

Kathalingam A, Senthilkumar V, Valanarasu S and Rhee JK 2012 Shape-Dependent Electrical Property of Solution Synthesized ZnO Nanorods. *Semiconduct.*

Sci. Technol. 27 (10).

Karajz D, Cseh D, Parditka B, Erdélyi Z and Szilágyi I 2022 Combining ZnO inverse opal and ZnO nanorods using ALD and hydrothermal growth. *J Therm Anal Calorim.* 147: 10259–10265.

Kennedy OW, White ER, Shaffer MSP and Warburton PA 2019 Vapour-liquid-solid growth of ZnO-ZnMgO core -shell nanowires by gold-catalysed molecular beam epitaxy. *Nanotechnology.* 30: 194001.

Khayatian A, Asgari V, Ramazani A, Akhtarianfar SF, Kashi MA and Safa S 2017 Diameter-Controlled Synthesis of ZnO Nanorods on Fe-Doped ZnO Seed Layer and Enhanced Photodetection Performance. *Mater. Res. Bull.* 94: 77–84.

Kim KH, Utashiro K, Abe Y and Kawamura M 2014 Growth of Zinc Oxide Nanorods Using Various Seed Layer Annealing Temperatures and Substrate Materials. *Int. J. Electrochem. Sci.* 9: 2080–89.

Kong X, Wei C, Zhu Y, Cohen P and Dong J 2018 Characterization and Modeling of Catalyst-free Carbon-Assisted Synthesis of ZnO Nanowires. *Journal of Manufacturing Processes.* 32: 438–444.

Liu Y, Hua L, Shuangqing L, Guoxi X and Xing X 2011 Synthesis and Characterisation of ZnO Microstructures via a Cationic Surfactant-Assisted Hydrothermal Microemulsion Process. *Mater. Characteris..* 62 (5): 509–16.

Liu Y and Gao W 2015 Growth process, crystal size and allignment of ZnO nanorods synthesised under neutral and acidic conditions. *J. Alloys Compd.* 629: 84–91.

Malevu TD, Mwankemwa BS, Ahamed MAM, Motaung TE, Tshabalala KG and Ocaya RO 2019 Effect of Ni Doping on ZnO Nanorods Synthesized Using a Low-Temperature Chemical Bath. *Journal of Electronic Materials.* 48 (11): 6954-6963.

Mohamed R, Rouhi J, Malek MF, Ismail AS and Salman AHS, Khan HA, Khan HA, Khusaimi Z, Mamat MH and Mahmood MR 2016 Sol Gel Synthesised Zinc Oxide Nanorods on Single And Co- Doped ZnO Seed Layer Templates : Morphological , Optical and Electrical Properties. *Int. J. Electrochem. Sci* 11: 2197–2204.

Mohammad SM, Hassan Z, Abd-Alghafour NM, Ali AMA, Ahmed NM, Abdalrheem R, Yam FK and Afzal N 2020 Ultraviolet Electroluminescence from Flowers-like n-ZnO Nanorods/p-GaN Light-Emitting Diode Fabricated by Modified Chemical Bath Deposition. *J. Lumin.* 226: 117510.

Mosalagae K, Murape DM and Lepodise LM 2020 Effects of Growth Conditions on Properties of CBD Synthesised ZnO Nanorods Grown on Ultrasonic Spray Pyrolysis Deposited ZnO Seed Layers. *Heliyon* 6 (7): e04458.

Mwankemwa BS, Malevu TD, Sahini MG and Vuai SA 2022 Effects of Vertically Aligned ZnO Nanorods Surface Morphology on the Ambient-Atmosphere Fabricated Organic Solar Cells. *Results Mater.* 14: 100271.

Mufti N, Maryam S, Fibriyanti AA, Kurniawan R, Fuad A, Taufiq A and Sunaryono 2018 Morphological Modification and Analysis of ZnO Nanorods and Their Optical Properties and Polarisation. *Scanning*, 2018.

Nandanapalli KR and Mudusu D 2018 Surface Passivated Zinc Oxide (ZnO) Nanorods by Atomic Layer Deposition of Ultrathin ZnO Layers for Energy Device Applications. *ACS Appl. Nano Mater.* 1(8): 4083–4091.

Narayanan GN, Ganesh RS and Karthigeyan A 2016 Effect of Annealing Temperature on Structural, Optical and Electrical Properties of Hydrothermal Assisted Zinc Oxide Nanorods. *Thin Solid Films* 598 (3): 39–45.

Pereira E, Chaves M, Junior G, Arruda LBD, Lisboa-filho PN, Durrant SF, Roberto J and Bortoleto R 2013 Al-Doping Effect on the Surface Morphology of ZnO Films Grown by Reactive RF Magnetron Sputtering. *Mater. Sci. Applicat.* 2013 (December): 761–67.

Rana AK, Kumar Y, Saxena N, Das R, Sen S and Shirage PM 2015 Studies on the Control of ZnO Nanostructures by Wet Chemical Method and Plausible Mechanism. *AIP Advances* 5 (9).

Shabannia R and Abu Hassan H 2014 Controllable vertically aligned ZnO nanorods on flexible polyethylene naphthalate (PEN) substrate using chemical bath deposition synthesis. *Appl. Phys. A.* 114: 579–584.

Shabannia R 2015 Vertically Aligned ZnO Nanorods on Porous Silicon Substrates: Effect of Growth Time. *Progr. Nat. Sci.: Mater. Int.* 25 (2): 95–100.

Shabannia R 2016 Effects of Growth Duration and Precursor Concentration on the Growth of ZnO Nanorods Synthesised by Chemical Bath Deposition. *Iran J. Sci. Technol. Trans: Sci.* 40 (1): 19–25.

Solís D, Martín J, Schrebler R, Navarrete-Astorga E, López-Escalante MC, Peinado-Pérez JJ, Ramos-Barrado JR and Dalchiele EA 2020 Electrochemical growth of ZnO nanorod arrays onto transparent conductive IZO:Ga substrates *J. Electrochem. Soc.* 167 112504.

Singh N, Kumar L, Kumar A, Vaisakh S, Singh SD, Sisodiya K, Srivastava S, Kansal M, Rawat S, Singh TA, Tanya, Anita 2017 Fabrication of Zinc Oxide/ Polyaniline (ZnO/PANI) Heterojunction and Its Characterisation at Room Temperature. *Mater. Sci. Semiconduct. Process.* 60: 29–33.

Strano V, Greco MG, Ciliberto E and Mirabella S 2019 ZnO Microflowers Grown by Chemical Bath Deposition: A Low-Cost Approach for Massive Production of Functional Nanostructures. *Chemosensors* 2019, *7*(4), 62

Strelchuk V, Kolomys O, Rarata S, Lytvyn P, Khyzhun O, Chey CO, Nur O and Willander M 2017. Raman Submicron Spatial Mapping of Individual Mn-Doped ZnO Nanorods. *Nanoscale Res. Lett.* 12.

Sze SM 1979 Physics of Semiconductor Devices, 3rd ed, Wiley, New York.

Ungula J, Kiprotich S, Swart HC and Dejene BF 2022 Investigation on the material properties of ZnO nanorods deposited on Ga-doped ZnO seeded glass substrate: Effects of CBD precursor concentration. *Surf Interface Anal.* 54: 1023–1031.

Vallejos S, Pizúrová N, Gràcia I, Sotelo-Vazquez C, Čechal J, Blackman C, Parkin I and Cané Carles 2016 ZnO Rods with Exposed {100} Facets Grown via a Self-Catalyzed Vapor-Solid Mechanism and Their Photocatalytic and Gas Sensing Properties. *ACS Appl. Mater. Interfaces.* 8: 33335−33342.

Xu S and Wang ZL 2011 One-dimensional ZnO nanostructures: Solution growth and functional properties. *Nano Res.* 4: 1013–1098.

Yuan Z 2015 Low-Temperature Growth of Well-Aligned ZnO Nanorod Arrays by Chemical Bath Deposition for Schottky Diode Application. *J. Electron. Mater.* 44: 1187–1191.

Yao C, Lin J, Qu Y, Jiang K, Hu Z, Li L, Xu N, Sun J, and Wu J 2022 WS_2-Decorated ZnO Nanorods and Enhanced Ultraviolet Emission. *Mater. Lett.* 306: 130880.

Zhitao H, Sisi L, Jinkui C and Yong C 2013 Controlled Growth of Well-Aligned ZnO Nanowire Arrays Using the Improved Hydrothermal Method. *J. Semiconduct.* 34 (6): 063002.